ACS OMEGA

Article

Cite This: ACS Omega 2018, 3, 5846−5852

Improvement of Laser-Crystallized Silicon Film Quality via Intermediate Dielectric Layers on a Glass Substrate

Kamil ÇINAR,*[,†,‡] Mehmet KARAMAN,[‡] and Alpan BEK[†,‡,§]

[†]Physics Department, [‡]The Center for Solar Energy Research and Applications (GÜNAM), and [§]Micro and Nanotechnology Program, Middle East Technical University, Dumlupınar Blvd. 1, 06800 Ankara, Turkey

ABSTRACT: The laser crystallization (LC) of amorphous silicon thin films into polycrystalline silicon (pc-Si) thin films on glass substrates is an active field of research in the fabrication of Si-based thin film transistors and thin film solar cells. Efforts have been, in particular, focused on the improvement of LC technique. Adhesion promoters of the crystallized Si thin films at the glass interface play a crucial role in the stability and device performance of fabricated structures. The crystalline Si thin films are required to be produced free of contamination risks arising from impurity diffusion from the glass substrate. Moreover, it is preferable to fabricate pc-Si thin films at temperatures as close as possible to the ambient temperature for an effective cost reduction. In this work, we demonstrate the successful use of a commercially available nanosecond pulsed laser marker at 1064 nm wavelength for Si crystallization at ambient conditions compared to the common method of pre-elevated substrate temperatures used in continuous wave laser irradiation technique. As a result, our technique results in a better energy balance than that in previous works. The second main purpose of this study is to enhance the crystallinity of Si thin films and to determine the best choice of an intermediate dielectric layer (IDL) comparatively among four thin buffer layers, namely, SiN_x, SiO_2, ZnO, and TiO_2, for the sake of obtaining improved adhesion and larger crystalline domains as compared to that on a direct Si−glass interface. The crystalline qualities of samples containing IDLs of SiN_x, SiO_2, ZnO, and TiO_2 were compared via Raman spectroscopy analysis and electron backscatter diffraction method against the direct Si−glass interface reference. The analyses quantitatively showed that both the crystallinity and the domain sizes can be increased via IDLs.

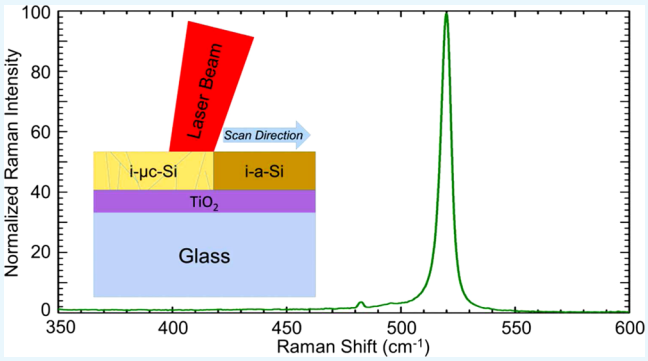

INTRODUCTION

Obtaining polycrystalline silicon (pc-Si) thin films via in situ annealing of amorphous silicon (a-Si) films on various carrier substrates is attractive for electronics industry, especially for Si-based thin film transistors and solar cell applications.[1,2] Particularly, cost-effective glass substrates are the most prevalent materials for the crystallization of a-Si. The traditional way of producing pc-Si thin films is the solid-phase crystallization (SPC) method. However, SPC method has drawbacks of long annealing durations (∼24 h) and small grain size (∼1−3 μm), which result in high defect concentrations.[3,4] Rapid thermal annealing (RTA) is also a SPC method in which typically a halogen lamp is used to heat and crystallize a-Si thin films over glass substrates.[5] The RTA process starts with a steep heating ramp (∼200 °C/s), which is followed by a steady temperature phase of ∼900 °C and finalizes with a cooling down (∼80 °C/s) phase, all maintained under an appropriate gas ambient.[5] During these stages of the process, deformations occur on the glass substrates, which limits the choice of substrate materials.[5] Aluminum-induced crystallization (AIC) of a-Si is another crystallization method that is carried out at relatively lower temperatures (<500 °C), and grain sizes (>10 μm) achieved using this method makes AIC pc-Si films suitable as seed layers for further crystallization techniques.[6] Besides, the use of different intermediate dielectric layers (IDLs; such as SiN_x, SiO_2, ZnO, and TiO_2) can change the pc-Si film properties such as grain orientation and grain size.[6,7] The subsequent epitaxial growth on AIC seed layers was studied extensively.[8,9] However, although resulting in large grains, the high density of intragrain defects makes this method inconvenient for solar cell applications.[10,11] The liquid-phase crystallization (LPC) is an alternative way of producing pc-Si films. A deposited thin a-Si layer on glass is locally melt by a focused energy source such that the rapid off-switching of the energy inflow results in a quick solidification after which a-Si ends up as pc-Si. LPC by electron beam (e-beam) crystallization of Si is used to produce pc-Si layers up to 10 μm in thickness on glass substrates.[12−15] Furthermore, LPC was improved by using a line-shaped e-beam source.[15] In previous studies, it was shown that LPC method resulted in more efficient thin film pc-Si solar cells.[13−17]

In addition to e-beam crystallization method, laser crystallization (LC) is another method for use in LPC.[5,13,15,16,18−22] Especially, by using a continuous wave

Received: March 20, 2018
Accepted: May 16, 2018
Published: May 30, 2018

DOI: 10.1021/acsomega.8b00530
ACS Omega 2018, 3, 5846−5852

(CW) laser in LPC, crystalline domain size in the range of millimeters in width and up to centimeters in length on glass substrates was achieved.[13,20,22] Moreover, the defects and deformations of the substrates can be avoided or lowered and the choice of substrates and IDLs (buffer layers) can be diversified.[12,16,19,21,23,24] The LC method for crystallization of a-Si thin films was studied with CW diode lasers with a line-focus in which the axis of the line-focus was perpendicular to scan directions.[24,25] Most of the past work was carried out using CW infrared (IR) lasers, and a-Si films on glass substrates were kept at elevated temperatures during the laser annealing process because at room temperature the a-Si layers exhibit low absorption of the infrared irradiation in comparison to the visible.[5,24] To increase the light absorption, the samples were kept at temperatures in the range of 400−700 °C.[5,12−14,16,18] Besides the absorption enhancement, the thermal expansion coefficient of the glass substrates approaches to that of crystalline silicon (c-Si) at around 600 °C.[22] Additionally, the elevated substrate temperature can be used to avoid the crack formation through crystalline domains during the LC process and it can reduce thermally induced stress on the pc-Si layers.[5,16,22,24]

Importance of an IDL between the glass substrate and the pc-Si thin film is attributed to its features such as blocking the diffusion of contaminants from the substrate into the pc-Si film during thermal processes and preventing lattice or average interatomic distance mismatch between the substrate and the film.[6,15,16,19] For LPC, c-Si/SiO_2 nanocrystalline interface with an undefined stoichiometry was observed.[26] LPC process by e-beam with an interface of SiO_2 was found to be suitable as an IDL between the glass substrate and the silicon thin film, which improved the homogeneity of the thickness of the crystallized absorber.[26] Besides using SiO_2 as an IDL, SiN_x can be an alternative. The amount of Si content in SiN_x layers can change the crystallization properties of the a-Si films; moreover, the quality of pc-Si films can be improved by a SiN_x IDL. For example, such a layer can be deposited by decreasing the NH_4/SiH_4 ratio, that is, increasing silicon in the content of the SiN_x IDL[6] in a plasma-enhanced chemical vapor deposition (PECVD) system. It was also shown that SiN_x IDLs with a higher Si content helped in the improvement of the crystallinity of Si thin films more than that of the samples with IDLs of Al/ZnO (AZO).[6] In the study of Dore et al.,[13] SiC_x was shown to act as a better wetting layer than SiO_2 or SiN_x. Besides that, there was no correlation between laser fluence and crystallinity of the pc-Si layer.[13] It was shown that SiO_2 IDL provided larger crystal grains of Si induced by the laser irradiation than that of SiN_x because the thermal conductivity of SiO_2 is lower than that of the glass substrate.[27,28] Thus, the best heat flow decreases from the Si film; on the contrary, the SiN_x layer has a higher thermal conductivity than that of SiO_2, which makes the Si film lose the heat during the laser-induced LPC.[27,28]

In this work, LPC of a-Si was performed by a 1064 nm nanosecond pulsed laser with different types of IDLs in between e-beam-deposited a-Si and a glass substrate. While LC processing of a-Si films, the effects of the varied IDLs were investigated quantitatively by Raman spectroscopy and qualitatively by electron backscatter diffraction (EBSD) and scanning electron microscopy. Compared to CW lasers, the pulsed laser enabled the process to increase the energy efficiency of the fabrication of a-Si thin films on glass by nullifying the cost of extra preheating of the substrates up to a temperature of 700 °C. It was shown that a commercially available 1064 nm nanosecond laser marker, which was originally not tailored for this specific purpose, can actually be a convenient tool. The IDLs of SiN_x, SiO_2, ZnO, and TiO_2, deposited on glass substrates separately, were investigated and compared with each other as well as a reference sample without an IDL in relation to the crystallinity quality of the Si thin films in the aspects of Raman and EBSD analyses.

EXPERIMENTAL SECTION

Preparation of Thin Films. In all of the experiments, Schott AF 32 Eco glass with a thickness of 1.1 mm was used as a substrate. The glass were cleaned in an ultrasonic bath with acetone, isopropanol, and distilled water for 10 min in each step. Finally, the glass were dipped into 10% hydrofluoric acid solution for 15 s and then cleaned with distilled water. Four different IDLs, SiN_x, SiO_2, ZnO, and TiO_2, were deposited before a-Si deposition. SiN_x deposition was carried out by a PECVD system (Vaksis Guner), in which decomposition of ammonia (NH_3) and silane (SiH_4) precursor gases with a ratio of 1:2 NH_3/SiH_4 was used. We would like to note that all of the used PECVD deposition gases (Linde and Air Liquide) were of 99.999% purity. The gas pressure was kept at 1.3×10^2 Pa, and the substrate temperature (T_s) was kept at 200 °C. The final thickness of SiN_x was 30 nm. SiO_2 was deposited by reactive sputtering technique (Vaksis NanoD) with a fused silica target (99.995% purity, Kurt-Lesker). The gas pressure was kept at 0.53 Pa, and the ratio of Ar to O_2 was kept at 30. The substrate was not heated during the film deposition. The final thickness of SiO_2 was 30 nm. TiO_2 layers were deposited by atomic layer deposition (ALD, Vedge ALD). At the system pressure of 30 Pa, the flow rate of the precursor N_2 was 20 sccm, whereas the pressures of the precursors for O_2 and Ti were 50 and 40 Pa, respectively. The substrate temperature was 130 °C, and 550 ALD cycles were performed. The cycles proceeded as follows: 15 ms for Ti precursor (tetrakis(dimethylamido)titanium, Sigma-Aldrich, 99.999% purity) injection, 15 s for purge, 15 ms for O_2 injection, and 15 s for purge consecutively. The final thickness of TiO_2 was 30 nm. ZnO layers were also deposited by ALD: 15 ms Zn precursor (diethylzinc, Sigma-Aldrich, deposition systems grade) injection, 5 s N_2 purge, 15 ms H_2O injection, and 15 s N_2 purge consecutively. 200 ALD cycles were performed at 200 °C, resulting in a thickness of ∼30−35 nm ZnO layer. After the buffer layer processes were accomplished, an a-Si thin film was deposited onto each IDL. E-beam (Vaksis EC e-Beam) evaporation was used for a-Si deposition. For the evaporation of Si, the base pressure of the chamber was 2.66×10^{-5} Pa, and during the deposition, the pressure was kept between 1×10^{-4} and 6.6×10^{-5} Pa. The substrate temperature was kept constant at 250 °C during the evaporation process, and e-beam current was varied between 100 and 115 mA to keep the deposition rate constant at 1 nm/s. The thickness of the a-Si layer was ∼600 nm for all samples.

Laser Crystallization Procedure. In this work, a 1064 nm wavelength nanosecond pulsed laser was employed. The duration of the pulses was measured as 200 ns via a fast Si photo detector. The value of the pulse duration is given as the full width at half-maximum (FWHM) value of the measured pulse in time. The pulse repetition rate was 80 kHz. The average power of the irradiation at the surface of the samples was 1.32−1.53 watt, and the pulse energy was 16.5−19.1 μJ. The effective laser focal spot diameter on the Si thin films was ∼40 μm so that the peak fluence of the laser on the thin films corresponded to a value of 2.63−3.04 J/cm^2. The peak fluence

DOI: 10.1021/acsomega.8b00530
ACS Omega 2018, 3, 5846−5852

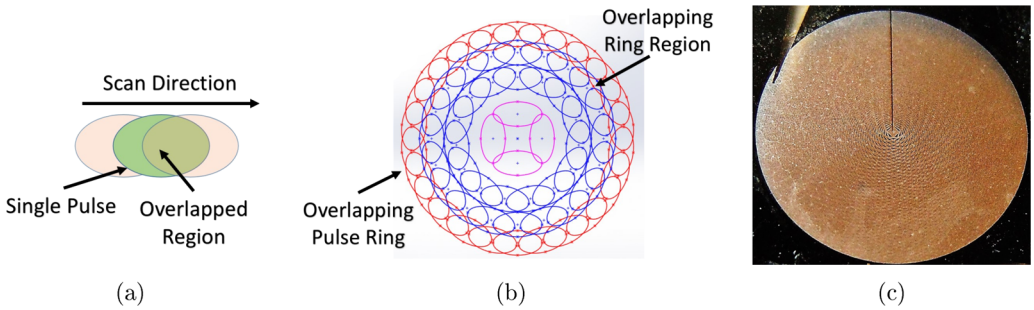

Figure 1. LC processing of samples: (a) pulse-overlap, (b) ring-overlap, and (c) photograph of the LC-processed pc-Si disk with a diameter of 12 mm.

was adjusted to keep the extinct energy in the a-Si film constant according to the variations in the thicknesses of the samples. The scan speed was set at a value of 114.4 mm/s, which maintained the pulse-overlap ratio at a value of 97.6%. At this scan speed, LC processing of a 1 cm^2 area takes about 25 s. The laser focus was scanned on the samples in a pattern of concentric rings forming a continuous disk (Figure 1). In addition to the overlapping of successive pulses, the concentric rings are also maintained to overlap with increasing diameter.

The samples were processed and characterized in quintuplicate for obtaining statistics as the fabrication is prone to variations due to uncertainties in the leveling of the sample substrates, the jitter in the laser system, and so forth. All samples were analyzed using Raman spectroscopy to check the consistency of the laser process, measured at a similar location on each sample, which is approximately midway between the center and the circumference of the disk.

RESULTS AND DISCUSSION

Raman Spectroscopy. For the analysis of crystallinity, Raman spectroscopy was used with a CW solid state laser at a wavelength of 532 nm as the excitation source. For each sample, the crystalline Si Raman shift frequency of the phonon peak center around 521 cm^{-1} and FWHM value of each peak were measured via a 50 cm monochromator ICCD-based fiber-coupled Raman spectroscopy system (Horiba-JobinYvon iHR550). A calibration was performed before each measurement using a c-Si sample by monitoring the one-phonon peak at 521 cm^{-1} with a FWHM value of ≈3.8 cm^{-1} to ensure consistency (see Figure 2). To minimize instrumental errors, a spectrum of the reference c-Si sample was acquired before and after the measurements of each sample set to check for the proper calibration. The intensities of all Raman signals were normalized to make comparative deductions for samples in terms of peak position and peak width easily. Having determined the Raman peak positions and the FWHM values for the same type of samples, the average values and variations were calculated (see Figure 3).

The Raman peak position of the sample without a buffer layer exhibited a red shift more than that of other samples, which indicates a higher tensile stress than that of others. This can be attributed to the mismatch of the thermal conductivities and the thermal expansion coefficients of the glass substrate and laser-induced pc-Si. The corresponding crystalline grain sizes are given in Table 1. The narrowed Raman peaks for the ZnO and TiO_2 samples point out larger single crystal domain sizes and hence a better crystallinity in the processed regions than that of the other samples. In Figure 3, it can be seen from the Raman peak positions that the average tensile stress

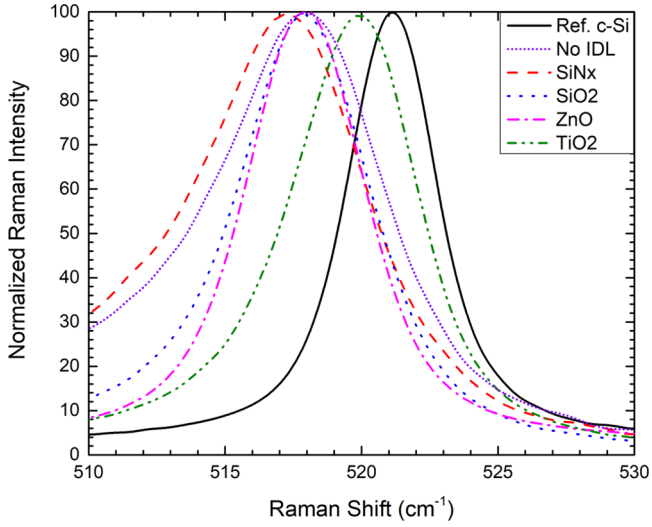

Figure 2. Average Raman spectra of the IDL sample sets.

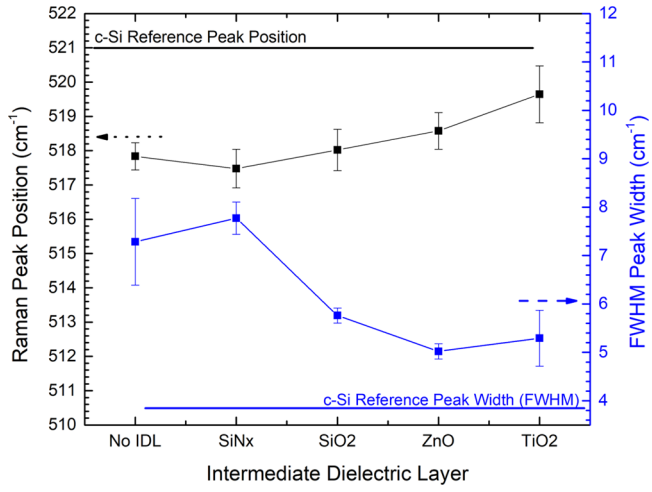

Figure 3. Comparison of Raman peak positions and peak widths.

decreases gradually for the samples with SiO_2, ZnO, and TiO_2 IDLs, respectively. The variation in the values of TiO_2 restrains us to compare it safely with the values of SiO_2 and ZnO. It can be deduced that the samples with SiO_2, ZnO, and TiO_2 IDLs are promising for achieving good crystallinity by pulsed IR laser-based LC. The thermal conductivity of SiN_x lying between 20 and 70 W/m/K[29] is considerably higher than that of SiO_2 (1.14−1.31 W/m/K[30]) and TiO_2 (6.5−8.5 W/m/K[31]). It is expected for SiN_x to transfer the generated heat due to laser

DOI: 10.1021/acsomega.8b00530
ACS Omega 2018, 3, 5846−5852

Table 1. Thermal Conductivities of IDLs

material type	thermal conductivity (W/m/K)	mean grain size (μm)	Raman peak position (cm^{-1})
Schott AF 32 Eco glass	1.16	0.24	517.8
SiN_x	20−70	0.27	517.5
SiO_2	1.14−1.31	0.55	518.0
ZnO	4 (at 1000 °C)−37	1.01	518.6
TiO_2	6.5−8.5	0.41	519.6

pulse absorption in a-Si to the glass substrate without resulting in as high local temperature increase and as high number of nucleation centers at the a-Si layer as compared to SiO_2 and TiO_2 (see Table 1).

Thermal conductivity of ZnO, about 37 W/m/K at room temperature, depends strongly on temperature and drops below 4 W/m/K at a temperature of 1000 °C[32] to a range comparable to those of SiO_2 and TiO_2. As can be seen in Table 1, mean grain sizes of the samples with SiO_2, ZnO, and TiO_2 are larger than those of bare glass and SiN_x IDL, whereas the tensile stresses are lower, as can be expected from Raman peak positions (see also Figure 3).

Electron Backscatter Diffraction. The samples were fine polished to remove any amorphous nanoscale layers on the surface before the inspection by EBSD. EBSD images were acquired on randomly chosen samples among the LC-processed sample sets.

As seen in Figure 4, there exists a variation in the grain sizes. The grain size can exceed 2 μm in length for the samples with TiO_2 and ZnO IDLs.

Augmentation of the grain sizes can be predicted from the red shift of the Raman peaks. An inverse correlation between the grain size and the red shift of the Raman peak was observed, as in reference.[33] The decreasing grain sizes address an increase in the tensile stress over the domains, in which this results in a red shift of transverse optical modes in the one-phonon Raman peak.[33−36] The biaxial tensile strain with an in-plane stress can be expressed as the following[35,37]

$$\Delta\omega = -4.0\sigma \text{ (GPa)}$$

where $\Delta\omega$ is the red shift in the Raman peak position of pc-Si with respect to the reference Raman peak position of c-Si (at ∼521 cm^{-1}) and the tensile stress is given as σ in GPa units. Accordingly, the tensile stress on the microcrystal domains takes values in between 0.1 and 0.9 GPa in our samples.

Secondary Ion Mass Spectroscopy (SIMS). As the a-Si film reaches melting temperatures, the generated heat inevitably diffuses to the underlying IDLs and glass substrate. Even solar glass substrates contain a considerable amount of impurity atoms that can migrate at elevated temperatures through the silica matrix and diffuse into the IDLs and crystallized Si layer. It is of importance to test whether the IDLs that are placed for thermal management can also function as diffusion barriers or whether they give rise to impurities in crystallized silicon themselves. To quantify these aspects, we have conducted secondary ion mass spectroscopy (SIMS) characterization of our samples (IONTOF TOF.SIMS[5]) after crystallization. SIMS analyses showed that the least impurity diffusion occurred in the sample with SiN_x IDL, whereas the other three showed a similar amount of impurity diffusion (see Figure 5). However, in the sample with SiN_x IDL, neither the measured Raman peak position nor the Raman peak FWHM is the closest to that of c-Si among all of the tested samples with IDLs, suggesting that the crystalline quality is not the best. It can be said that the thermal conductivities of IDLs turn out to be a more dominant factor in the achieved crystalline quality of the LC process.

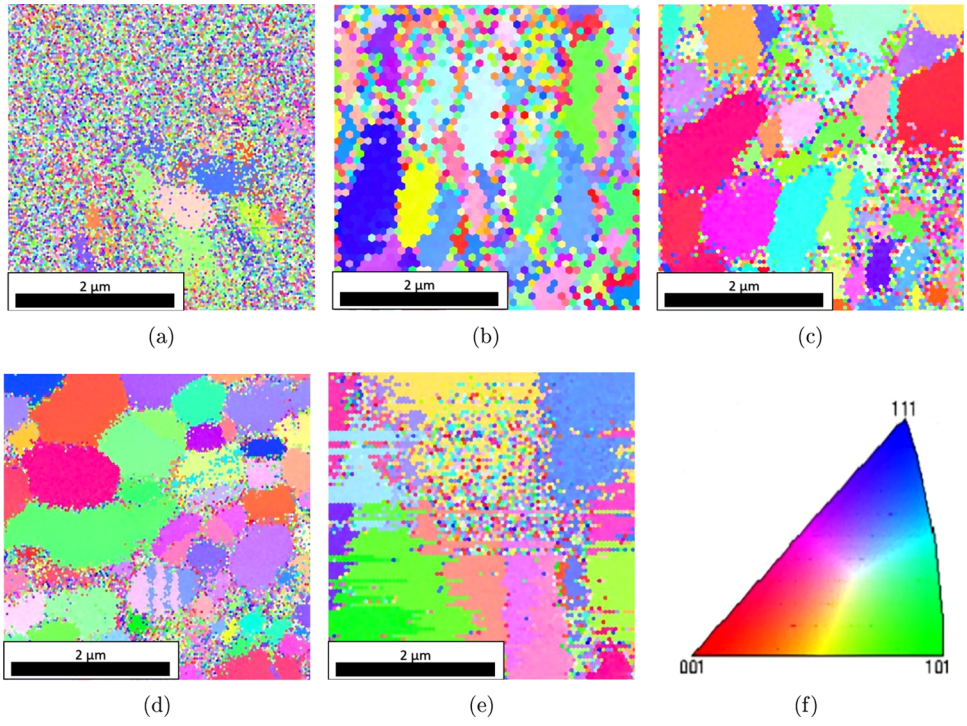

Figure 4. EBSD images of LC samples displaying microcrystal domains with (a) no IDL, (b) SiN_x, (c) SiO_2, (d) TiO_2, and (e) ZnO. Each color corresponds to a different crystal orientation. (f) Color map of crystal orientations of Si.

DOI: 10.1021/acsomega.8b00530
ACS Omega 2018, 3, 5846−5852

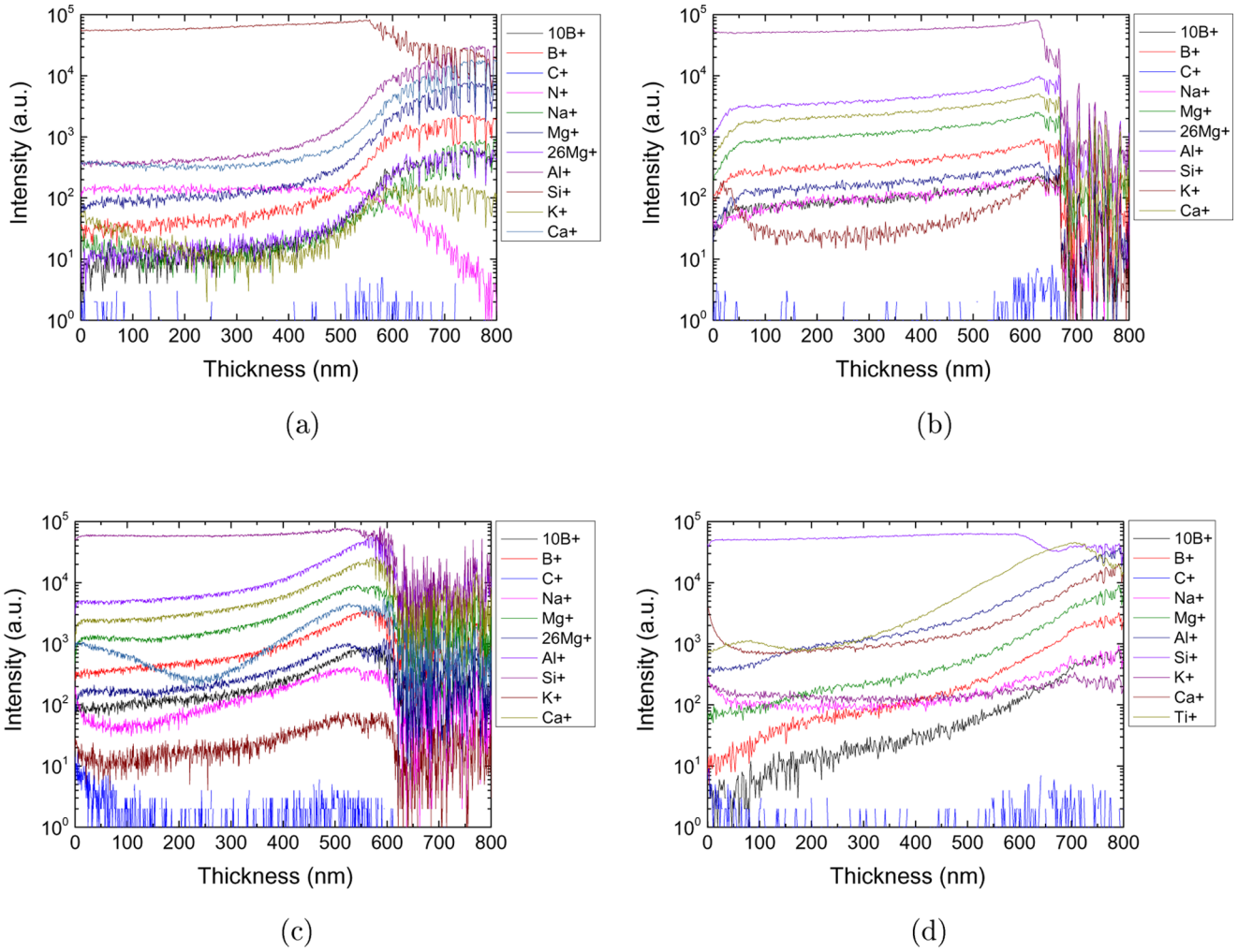

Figure 5. SIMS depth profile analyses of the samples with the IDLs (a) SiN_x, (b) SiO_2, (c) ZnO, and (d) TiO_2 for the concentration of common impurity atoms.

CONCLUSIONS

In laser-induced crystallization process of thin a-Si films, the samples with SiO_2, ZnO, and TiO_2 intermediate dielectric layers between the glass substrate and a-Si exhibit a better performance than that of the samples with SiN_x and the reference sample without IDL in terms of crystalline domain size, stress buildup, and defect concentration, as can be seen from EBSD domain analysis, Raman peak position, and Raman FWHM, respectively. Our understanding is that the heat can accumulate on irradiated areas with decreasing IDL thermal conductivity; consequently, the temperature can be maintained high long enough to enlarge the grains in size after the nucleation occurs. Such a correlation can be deduced by paying attention to the temperature dependence of the thermal conductivity of TiO_2 and ZnO IDLs (see Table 1). Expanding on that idea, one can suggest that as the cooling is slow in low thermal conduction, the resulting pc-Si domains are expected to contain less concentration of defects (or to be less amorphous), which is supported by lower Raman peak FWHM values observed in low thermal conductivity IDL samples. It can further be suggested from Table 1 that the samples with IDLs of ZnO and TiO_2 depict the formation of larger grains with less tensile stress because of more effective accumulation of heat and longer sustainment of elevated local temperature. Not only the crystal grains were increased in size with SiO_2, ZnO, and TiO_2 IDLs, but also the crystallinity of LC pc-Si was improved or amorphousness was reduced. Consequently, the tensile stress between the grains could be reduced to some extent with SiO_2, ZnO, and TiO_2 layers. Besides the thermal conductivity management, the IDLs may also function as diffusion barriers for the impurities originating from a glass substrate. Our SIMS studies have shown that SiN_x does function best as a diffusion barrier albeit it does not provide the best crystalline quality. We found that the magnitude of impurity diffusion is not as high to affect the crystalline quality adversely for the studied IDLs.

This work provides a quantitative comparison of the qualities of laser-induced crystallization products with different intermediate dielectric layers. Further studies have to be performed involving multi-intermediate layer performances, focal spot engineering, film thicknesses, and so forth, to assess the applicability of the method as a useful tool in obtaining crystalline Si thin films at device quality. We think that our findings will serve as a guide for future optimization studies on the laser crystallization of a-Si thin films and their applications.

AUTHOR INFORMATION

Corresponding Author

*E-mail: kcinar@metu.edu.tr. Tel: +903122104335.

DOI: 10.1021/acsomega.8b00530
ACS Omega 2018, 3, 5846−5852

ORCID
Kamil ÇINAR: 0000-0002-1192-6947
Alpan BEK: 0000-0002-0190-7945

Notes

The authors declare no competing financial interest.

■ ACKNOWLEDGMENTS

We thank Ezgi Aygün and Baran U. Tekin for their contributions in sample preparation and analyses, respectively. We also thank Middle East Technical University Central Laboratories for the EBSD study, especially Sedat Canlı. This work was supported by TÜBİTAK under grant no. 115M061 and METU BAP-08-11-2017-022.

■ REFERENCES

(1) Brotherton, S. D.; Ayres, J. R.; Young, N. D. Characterization of low temperature poly-Si thin film transistors. *Solid-State Electron.* **1991**, *34*, 671−679.
(2) Nast, O.; Puzzer, T.; Koschier, L. M.; Spproul, A.; Wenham, S. R. Aluminum-induced crystallization of amorphous silicon on glass substrates above and below the eutectic temperature. *Appl. Phys. Lett.* **1998**, *73*, 3214−3216.
(3) Song, D.; Inns, D.; Straub, A.; Terry, M. L.; Campbell, P.; Aberlee, A. G. Solid phase crystallized polycrystalline thin-films on glass from evaporated silicon for photovoltaic applications. *Thin Solid Films* **2006**, *513*, 356−363.
(4) Cielaszyk, E. S.; Kirmse, K. H. R.; Stewart, R. A.; Wendt, A. E. Mechanisms for polycrystalline silicon defect passivation by hydrogenation in an electron cyclotron resonance plasma. *Appl. Phys. Lett.* **1995**, *67*, 3099−3101.
(5) Slaoui, A.; Chowdhury, A.; Prathap, P.; Said-Bacar, Z.; Bahouka, A.; Mermet, F. Laser processing for thin film crystallization silicon solar cells. *Proc. SPIE* **2012**, *8473*, 84730C DOI: 10.1117/12.929208.
(6) Kahraman, M.; Özmen, O. T.; Sedani, S. H.; Özkol, E.; Turan, R. Effects of glass substrate coated by different-content buffer layer on the quality of poly-Si thin films. *Phys. Status Solidi A* **2016**, *213*, 3142−3149.
(7) Toko, K.; Nakata, M.; Okada, A.; Sasase, M.; Usami, N.; Suemasu, T. Influence of substrate on crystal orientation of large-grained Si thin films formed by metal-induced crystallization. *Int. J. Photoenergy* **2015**, *2015*, 1−7.
(8) Tüzün, Ö.; Slaoui, A.; Roques, S.; Ballutaud, D.; et al. Solid phase epitaxy on N-type polysilicon films formed by aluminium induced crystallization of amorphous silicon. *Thin Solid Films* **2009**, *517*, 6358−6363.
(9) Dogan, P.; Gorka, B.; Sieber, I.; Fenske, F.; Gall, S. Low-temperature epitaxy of silicon by electron beam evaporation. *Thin Solid Films* **2007**, *515*, 7643−7646.
(10) Gestel, D. V.; Gordon, I.; Bender, H.; Saurel, D.; Vanacken, J.; Beaucarne, G.; Poortmans, J. Intragrain defects in polycrystalline silicon layers grown by aluminum-induced crystallization and epitaxy for thin-film solar cells. *J. Appl. Phys.* **2009**, *105*, No. 114507.
(11) Gestel, D. V.; Dogan, P.; Gordon, I.; Bender, H.; Lee, K. Y.; Beaucarne, G.; Gall, S.; Poortmans, J. Investigation of intragrain defects in pc-Si layers obtained by aluminum-induced crystallization: comparison of layers made by low and high temperature epitaxy. *Mater. Sci. Eng., B* **2009**, *159−160*, 134−137.
(12) Dore, J.; Evans, R.; Schebert, U.; Eggleston, B. D.; Ong, D.; Kim, K.; Huang, J.; Kunz, O.; Keevers, M.; Egan, R.; Varlamov, S.; Green, M. A. Thin-film polycrystalline silicon solar cells formed by diode laser crystallisation. *Prog. Photovolt: Res. Appl.* **2013**, *21*, 1377−1383.
(13) Weizman, M.; Rhein, H.; Dore, J.; Gall, S.; Klimm, C.; Andra, G.; Schultz, C.; Fink, F.; Rau, B.; Schlatmann, R. Efficiency and stability enhancement of laser-crystallized polycrystalline silicon thin-film solar cells by laser firing of the absorber contacts. *Sol. Energy Mater. Sol. Cells* **2014**, *120*, 521−525.
(14) Weizman, M.; et al. Rear-side all-by-laser point-contact scheme for liquid-phase-crystallized silicon on glass solar cells. *Sol. Energy Mater. Sol. Cells* **2015**, *137*, 280−286.
(15) Haschke, J.; Amkreutz, D.; Frijnits, T.; Kuhnapfel, S.; Hanel, T.; Rech, B. Influence of barrier and doping type on the open-circuit voltage of liquid phase-crystallized silicon thin-film solar cells on glass. *IEEE J. Photovoltaics* **2015**, *5*, 1001−1005.
(16) Dore, J.; Varlamov, S.; Green, M. A. Intermediate layer development for laser-crystallized thin-film silicon solar cells on glass. *IEEE J. Photovoltaics* **2015**, *5*, 9−16.
(17) Gabriel, O.; et al. PECVD intermediate and absorber layers applied in liquid-phase crystallized silicon solar cells on glass substrates. *IEEE J. Photovoltaics* **2014**, *4*, 1343−1348.
(18) Kühnapfel, S.; Nickel, N. H.; Gall, S.; Klaus, M.; Genzel, C.; Rech, B.; Amkreuts, D. Preferential {100} grain orientation in 10 micrometer-thick laser crystallized multicrystalline silicon on glass. *Thin Solid Films* **2015**, *576*, 68−74.
(19) Amkreutz, D.; Barker, W. D.; Kuhnapfel, S.; Sonntag, P.; Gabriel, O.; Gall, S.; Bloeck, U.; Schmidt, J.; Haschke, J.; Rech, B. Liquid-phase crystallized silicon solar cells on glass: increasing the open-circuit voltage by optimized interlayers for n- and p-type absorbers. *IEEE J. Photovoltaics* **2015**, *5*, 1757−1761.
(20) Sonntag, P.; Haschke, J.; Kuhnapfel, S.; Gabriel, O.; Amkreutz, D.; Rech, B. Properties of liquid phase crystallized interdigitated back-contact solar cells on glass. *Energy Procedia* **2015**, *77*, 487−492.
(21) Haschke, J.; Amkreutz, D.; Korte, L.; Ruske, F.; Rech, B. Towards wafer quality crystalline silicon thin-film solar cells on glass. *Sol. Energy Mater. Sol. Cells* **2014**, *128*, 190−197.
(22) Andrä, G.; Bergmann, J.; Falk, F. Laser crystallized multicrystalline silicon thin films on glass. *Thin Solid Films* **2005**, *487*, 77−80.
(23) Taheri, M. L.; McGowan, S.; Nikolova, L.; Evans, J. E.; Teslich, N.; Lu, J. P.; LaGrange, T.; Rosei, F.; Siwich, B. J.; Browning, N. D. In situ laser crystallization of amorphous silicon: controlled nanosecond studies in the dynamic transmission electron microscope. *Appl. Phys. Lett.* **2010**, *97*, No. 032102.
(24) Chowdhury, A.; Bahouka, A.; Steffens, S.; Schneider, S.; Dore, J.; Mermet, F.; Slaoui, A. Laser anneling of thin film polycrystaline silicon solar cell. *EPJ Photovoltaics* **2013**, *4*, No. 45108.
(25) Dore, J.; Ong, D.; Egan, R.; Green, M. A.; Varlamov, S. Progress in laser-crystallized thin-film polycrystalline silicon solar cells: intermediate layers, light trapping, and metallization. *IEEE J. Photovoltaics* **2014**, *4*, 33−39.
(26) Amkreutz, D.; Haschke, J.; Haring, T.; Ruske, F.; Rech, B. Conversion efficiency and process stability improvement of electron beam crystallized thin film silicon solar cells on glass. *Sol. Energy Mater. Sol. Cells* **2014**, *123*, 13−16.
(27) Chen, Y. R.; Chang, C. H.; Chao, L. S. Modeling and experiment analysis in excimer-laser crystallization of amorphous Si films on a glass substrate with different buffer layers. *J. Am. Ceram. Soc.* **2007**, *90*, 688−692.
(28) Yeh, W. C.; Matsumura, M. Numerical calculation of excimer-laser-induced lateral-crystallization of silicon thin films. *Jpn. J. Appl. Phys.* **2001**, *40*, 492−499.
(29) Okamoto, Y.; Hirosaki, N.; Ando, M.; Munakata, F.; Akimune, Y. Effect of sintering additive composition on the thermal conductivity of silicon nitride. *J. Mater. Res.* **1998**, *13*, 3473−3477.
(30) Huang, S.; Ruan, X.; Zou, J.; Fu, X.; Yang, H. Thermal conductivity measurement of submicrometer-scale silicon dioxide films by an extended micro-Raman method. *Microsyst. Technol.* **2009**, *15*, 837−842.
(31) Maekawa, T.; Kurosaki, K.; Tanaka, T.; Yamanaka, S. Thermal conductivity of titanium dioxide films grown by metal-organic chemical vapor deposition. *Surf. Coat. Technol.* **2008**, *202*, 3067−3071.
(32) Olorunyolemi, T.; Birnboim, A.; Carmel, Y.; Wilson, O. C.; Lloyd, I. K.; et al. Thermal conductivity of zinc oxide: from green to sintered state. *J. Am. Ceram. Soc.* **2004**, *85*, 1249−1253.
(33) Wei, W.; Xu, G.; Wang, J.; Wang, T. Raman spectra of intrinsic and doped hydrogenated nanocrystalline silicon films. *Vacuum* **2007**, *81*, 656−662.

DOI: 10.1021/acsomega.8b00530
ACS Omega 2018, 3, 5846−5852

(34) Jin, J.; Yuan, Z.; Huang, L.; Chen, S.; Shi, W.; Cao, Z.; Lou, Q. Laser crystallization of amorphous silicon thin films investigated by Raman spectroscopy and atomic force microscopy. *Appl. Surf. Sci.* **2010**, *256*, 3453−3458.
(35) Georgi, C.; Hecker, M.; Zschech, E. Effects of laser-induced heating on Raman stress measurements of silicon and silicon-germanium structures. *J. Appl. Phys.* **2007**, *101*, No. 123104.
(36) Kouteva-Arguirova, S.; Arguirov, T.; Wolfframm, D.; Reif, J. Influence of local heating on micro-Raman spectroscopy of silicon. *J. Appl. Phys.* **2003**, *94*, 4946−4949.
(37) Wolf, I. D. Micro-Raman spectroscopy to study local mechanical stress in silicon integrated circuits. *Semicond. Sci. Technol.* **1996**, *11*, 139−154.

DOI: 10.1021/acsomega.8b00530
ACS Omega 2018, 3, 5846−5852